

DISCOVERY OF STAR FORMATION IN THE EXTREME OUTER GALAXY POSSIBLY INDUCED BY A HIGH-VELOCITY CLOUD IMPACT

NATUKO IZUMI^{1,2}, NAOTO KOBAYASHI¹, CHIKAKO YASUI², ALAN T. TOKUNAGA³, MASAO SAITO^{4,5},
 AND SATOSHI HAMANO^{1,2}

Draft version November 27, 2014

ABSTRACT

We report the discovery of star formation activity in perhaps the most distant molecular cloud in the extreme outer galaxy. We performed deep near-infrared imaging with the Subaru 8.2 m telescope, and found two young embedded clusters at two CO peaks of “Digel Cloud 1” at the kinematic distance of $D = 16$ kpc (Galactocentric radius $R_G = 22$ kpc). We identified 18 and 45 cluster members in the two peaks, and the estimated stellar densities are ~ 5 and ~ 3 pc⁻², respectively. The observed K -band luminosity function suggests that the age of the clusters is less than 1 Myr and also that the distance to the clusters is consistent with the kinematic distance. On the sky, Cloud 1 is located very close to the H I peak of high-velocity cloud Complex H, and there are some H I intermediate velocity structures between the Complex H and the Galactic disk, which could indicate an interaction between them. We suggest the possibility that Complex H impacting on the Galactic disk has triggered star formation in Cloud 1 as well as the formation of the Cloud 1 molecular cloud.

Subject headings: Galaxy: formation – infrared: stars – ISM: clouds – stars: formation

1. INTRODUCTION

The extreme outer galaxy (EOG), which we define as the region with a Galactocentric radius (R_G) of more than 18 kpc (Kobayashi et al. 2008; Yasui et al. 2008), has a very different environment from the solar neighborhood with a much lower gas density (Wolfire et al. 2003), lower metallicity (Smartt & Rolleston 1997), and little or no perturbation from the spiral arms. Such a region not only defines the size and shape of our Galaxy, but it also serves as an excellent laboratory for studying the star-forming process in low-density and low-metallicity environments. Because such environments may have similar characteristics that existed in the early phase of Galaxy formation (Kobayashi et al. 2008), we might be able to directly observe the galaxy formation processes in unprecedented detail at a much closer distance than distant galaxies.

The Digel Clouds were discovered by the very first survey of molecular clouds in the EOG (Digel et al. 1994) and are some of the best targets for studying star formation in the EOG. The Digel Clouds are composed of eight molecular clouds (Cloud 1–8), and R_G is estimated at more than 20 kpc for many of them from the kinematic distance. A star-forming region has been identified in Cloud 2 (de Geus et al. 1993; Kobayashi & Tokunaga 2000; Yasui et al. 2006, 2008), which has the highest CO luminosity among all Digel Clouds. These clouds are a very valuable sample, because the expected number

of molecular clouds in such a low-density region is very small (Snell et al. 2002).

In this paper, we report the discovery of star-forming clusters in Cloud 1, which has the largest dynamical mass among all of the Digel Clouds. Despite a relatively strong ¹³CO line, no star-forming activity has been reported thus far because of the very large distance with perhaps the largest Galactocentric radius ($R_G \approx 22$ kpc) among all known clouds in the Galaxy⁶. In view of the close coincidence on the sky with the high-velocity cloud (HVC) Complex H, we suggest that star and molecular cloud formation in Cloud 1 is triggered by HVC accretion onto the Galactic disk.

2. OBSERVATIONS AND DATA REDUCTION

2.1. Subaru MOIRCS Imaging

We obtained J (1.25 μ m)-, H (1.65 μ m)-, and K_S (2.15 μ m)-band deep images of the two CO peaks of Cloud 1 (Cloud 1a and Cloud 1b). The observations were conducted on 2006 September 2 UT with a wide-field near-infrared (NIR) camera, MOIRCS (Ichikawa et al. 2006) on the Subaru 8.2 m telescope. It provides a $4' \times 7'$ field of view with a $0''.117$ pixel⁻¹ scale and employs the Mauna Kea Observatory (MKO) NIR photometric filters (Tokunaga et al. 2002). The total integration time was ~ 700 , 600, and 600 s for J , H , and K_S bands, respectively. The observing condition was photometric and the seeing was excellent ($\sim 0''.4$) throughout the observing period.

2.2. Data Reduction

All of the data for each band were reduced with IRAF ver 2.14 with standard procedures: dark subtraction,

⁶ Although the kinematic distance of Cloud 2 is larger than that of Cloud 1 in Digel et al.’s (1994) original list, the photometric distance of Cloud 2 is found to be smaller than the kinematic distance ($R_G \approx 19$ kpc). See Section 4 for more detail.

¹ Institute of Astronomy, School of Science, The University of Tokyo, 2-21-1 Osawa, Mitaka, Tokyo 181-0015, Japan; izumi@ioa.s.u-tokyo.ac.jp

² Department of Astronomy, Graduate School of Science, The University of Tokyo, 7-3-1 Hongo, Bunkyo-ku, Tokyo 113-0033, Japan

³ Institute for Astronomy, University of Hawaii, 2680 Woodlawn Drive, Honolulu, HI 96822, USA

⁴ National Astronomical Observatory of Japan, 2-21-1 Osawa, Mitaka, Tokyo 181-8588, Japan

⁵ Joint ALMA Observatory, Ave. Alonso de Cordova 3107, Vitacura, Santiago, Chile

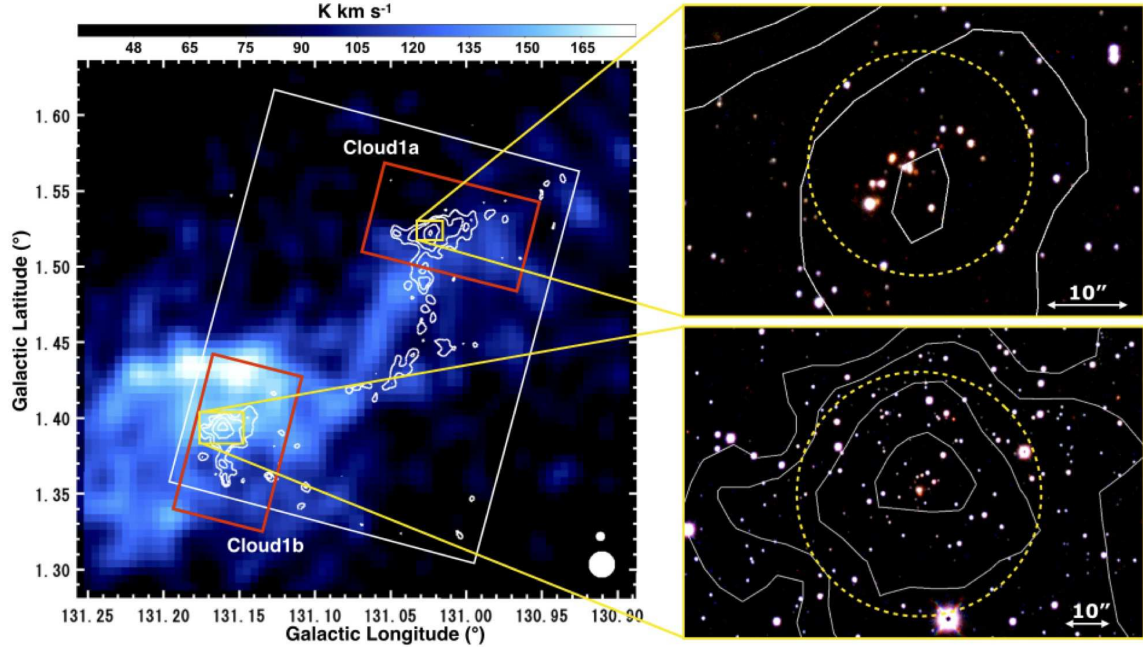


FIG. 1.— Left: H I map around Cloud 1 (from CGPS data : $v_{\text{LSR}} = -104.5 \sim -99.6 \text{ km s}^{-1}$). The white contours show the integrated ^{12}CO (1–0) map of Cloud 1 (from our NRO 45 m telescope data: $v_{\text{LSR}} = -104.1 \sim -99.1 \text{ km s}^{-1}$), and contour levels are at 2σ , 3σ , 5σ , 7σ ($1\sigma = 0.5 \text{ K km s}^{-1}$). The white and red boxes show the mapping size of the NRO 45 m observation and the field of view of the Subaru MOIRCS ($4' \times 7'$), respectively. The large and small white filled circles at the lower right corner show the beam sizes of the DRAO ($\sim 58''$) and NRO 45 m telescope ($\sim 17''$), respectively. Right: JHK pseudo color images of the Cloud 1 clusters from our Subaru MOIRCS data. The white contours show the same as the ^{12}CO map as in the left panel. The yellow dotted circles show the defined cluster regions (radius of Cloud 1a circle : $14''$, Cloud 1b : $28''$).

TABLE 1
PARAMETERS OF THE OBSERVATIONS CONTAINING THE REGION CLOUD 1 OR COMPLEX H

Project	Telescope	Wavelength	Coverage	Velocity Range (km s^{-1})	Velocity Resolution (km s^{-1})	Resolution ^a
CGPS	DRAO Synthesis Telescope	21.1 cm (H I)	$74^\circ.2 < l < 147^\circ.3$ $-3^\circ.6 < b < +5^\circ.6$	-150 to 50	1.32	$58'' \times 58'' \text{ cosec } \delta$
LAB survey	Villa Elisa 30 m	21.1 cm (H I)	$0^\circ < l < 360^\circ$ $-90^\circ < b < -25^\circ$	-450 to 450	1.27	$30'.0$
	Dwingeloo 25 m	21.1 cm (H I)	$0^\circ < l < 360^\circ$ $-30^\circ < b < +90^\circ$	-450 to 450	1.25	$35'.7$
FCRAO outer Galaxy Survey	FCRAO 14 m	2.6 mm (^{12}CO)	$102^\circ.49 < l < 141^\circ.54$ $-3^\circ.03 < b < +5^\circ.41$	-153 to 40	0.98	$45''$
WISE	WISE satellite	$3.4 \mu\text{m}$	All-sky	$6''.1$
		$4.6 \mu\text{m}$	All-sky	$6''.4$
		$12 \mu\text{m}$	All-sky	$6''.5$
		$22 \mu\text{m}$	All-sky	$12''.0$
IPHAS	Issac Newton 2.5 m (Wide Field Camera)	656.8 nm (H α)	$29^\circ < l < 215^\circ$ $-5^\circ < b < +5^\circ$	$0''.333 \text{ pixel}^{-1}$
This paper	Subaru 8.2 m (MOIRCS)	$1.25 \mu\text{m}$ (J)	$4' \times 7' \times 2$	$0''.112 \text{ pixel}^{-1}$
		$1.65 \mu\text{m}$ (H)	$4' \times 7' \times 2$	$0''.112 \text{ pixel}^{-1}$
		$2.15 \mu\text{m}$ (K_S)	$4' \times 7' \times 2$	$0''.112 \text{ pixel}^{-1}$
	NRO45 m	2.6 mm (^{12}CO)	$15' \times 16'$	-110 to -90	0.25	$\sim 17''$

NOTE. — ^a The meaning of the resolution with the IPHAS and Subaru 8.2 m observation is pixel size, and others is diffraction limited resolution.

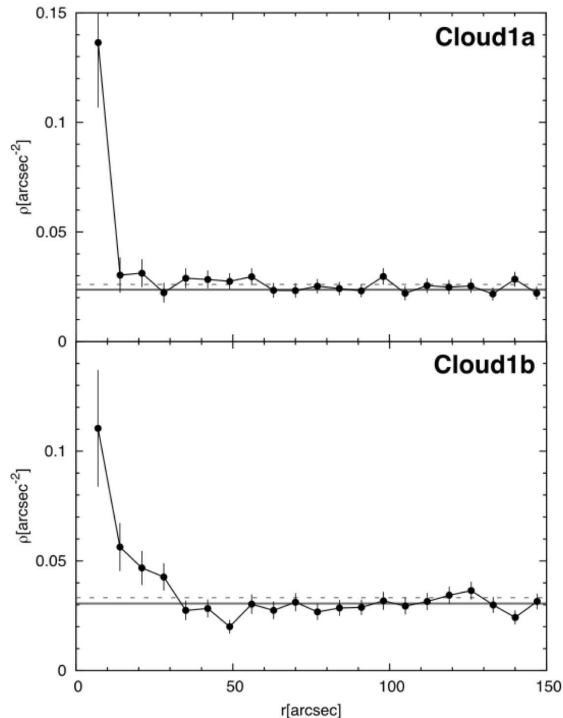


FIG. 2.— Radial variation of the projected stellar number density of stars around the center of the CO peaks. The center position of Clouds 1a and 1b are $(l, b) = (131^\circ.02, 1^\circ.52)$ and $(131^\circ.16, 1^\circ.39)$, respectively. The error bars represent Poisson errors (1σ). The horizontal solid lines and horizontal dashed lines indicate the average density of stars outside the Cloud 1 clouds and the Poisson errors (3σ), respectively.

flat fielding, bad-pixel correction, median-sky subtraction, image shifts with dithering offsets, and combining. The stellar FWHM in final images of the J , H , and K_S bands are $0''.45$, $0''.43$, and $0''.40$, respectively. JHK_S photometry has been performed using the IRAF APPHOT package, with aperture diameters of $1''.17$ (10 pixels). The aperture sizes were chosen to achieve high signal-to-noise ratio (S/N) and sufficient flux count from the stellar objects. Photometric calibration was done using the standard star Persson9166 (GSPC P330-E; $J = 11.772$, $H = 11.455$, $K = 11.419$; Leggett et al. 2006). The resultant 10σ limiting magnitudes in the J , H , and K_S bands were estimated at 21.0, 20.5, and 19.5 mag, respectively.

2.3. CO Data with the Nobeyama Radio Observatory (NRO) 45 m Telescope

We have performed observations of Cloud 1 in the CO ($J = 1-0$; 115.271 GHz) line with the NRO 45 m telescope⁷ in 2007 December. We used the 25-BEAM Array Receiver System (BEARS) in the double-side band mode, which has 5×5 beams separated by $41''.1$ on the plane of the sky (Sunada et al. 2000; Yamaguchi et al. 2000). The telescope beamwidth and the main beam efficiency at 115 GHz was $14''.5$ and 0.39, respectively. As a backend, the autocorrelator was adopted, and the typical noise level was 0.40 K in T_A^* with 0.25 km s^{-1} resolution in CO.

⁷ The Nobeyama Radio Observatory is a branch of the National Astronomical Observatory of Japan, National Institutes of Natural Sciences.

We employed an on-the-fly mode developed for the NRO 45 m telescope (Sawada et al. 2008). The data sampling interval of the R.A. or decl. scans is $\sim 1''$, and the separation between the each scans is $5''.1$. After subtracting linear baselines, the data were convolved with a Gaussian-tapered Bessel function whose FWHM was $14''$ and resampled onto a $6''$ grid. Since the telescope beam is a Gaussian with an FWHM of $14''.5$ – $14''.8$, and effective FWHM resolution of $\sim 17''$. Finally, to reduce the “scanning effect”, where some of the conditions outlined above have not been adequately satisfied, resulting in an effective noise level on the final map higher than the theoretical value, we combine the two maps scanned R.A. and decl. directions using the basket-weaving method (Emerson & Graeve 1988). We mapped an area of $15' \times 16'$ in CO to cover the entire Cloud 1 (Figure 1).

The atmospheric corrected temperature scale T_A^* is obtained with the chopper wheel method. During the observation, the typical system noise temperature of BEARS in the double-side band was 400 K at CO frequencies. The telescope pointing was checked about every 90 minutes by five-point scans of the SiO maser source S-Per [R.A. = $02^h 22^m 51^s.713$, decl. = $58^\circ 35' 11''$. 50 (J2000)] with SIS 49 GHz receiver (S40). The measured pointing errors ranged from $1''.5$ to $6''.0$ during the observing run.

2.4. Previous Observations

In addition to the our NIR and CO observation, we used archived data from previous observations “the Canadian Galactic Plane Survey (CGPS)” (Taylor et al. 2003), “the FCRAO outer Galaxy Survey” (Heyer et al. 1998), “the Leiden/Argentine/Bonn (LAB) Survey of Galactic H I” (Kalberla et al. 2005), “the Wide-field Infrared Survey Explorer (WISE) all sky survey” (Wright et al. 2010), and “the INT/WFC Photometric H α Survey (IPHAS)” (Drew et al. 2005). We summarize in Table 1 the observations we used to study Cloud 1 or Complex H in this paper.

3. RESULTS

3.1. Detection of Star-forming Regions in Cloud 1

In the false-color pictures (Figure 1), we found two star clusters of reddened stars, in the vicinity of the two CO peaks, Cloud 1a and 1b (Digel et al. 1994). We examined the positional relationship between these clusters, Cloud 1, and the other foreground molecular clouds on the sky to confirm that Cloud 1 is the only molecular cloud positionally coincident with the clusters. Therefore, we concluded that these clusters are embedded clusters associated with Cloud 1. In view of the location of the clusters in the molecular clouds, near the peak of the dense CO core, these clusters are likely to be younger than $\sim 3 \text{ Myr}$ (Lada & Lada 2003).

In order to define the extent of the clusters, we derived the stellar number density distribution around the CO peaks (Figure 2). As a result, we defined the radius of the Cloud 1a and 1b cluster region to be $14''$ and $28''$, respectively.

3.2. Identification of Cluster Members

We identified cluster members using the $J - K_S$ versus J color-magnitude (CM) diagram of all the detected

sources with $S/N > 5\sigma$ in all three bands (Figure 3) following the method used in Yasui et al. (2006, 2008). On the CM diagram, we estimated the nominal extinction (A_V) of all the detected sources by measuring the distance along the reddening vector (Rieke & Lebofsky 1985) from a reference isochrone of an assumed age of 1 Myr and a kinematic distance of $D = 16$ kpc (see Figure 3). We found that stars with large extinction, $A_V \geq 4$ mag and 3 mag are concentrated on the Cloud 1a and Cloud 1b cluster area, respectively, while stars with small extinction ($A_V = 0\text{--}2$ mag) are uniformly distributed over the observed field (see insets in Figure 3). Therefore, we identified the cluster members with the following criteria: (1) distributed in the regions of Cloud 1a and Cloud 1b cluster region (see Figure 1) and (2) $A_V \geq 4$ and 3 mag for Cloud 1a and Cloud 1b, respectively. With this 2nd criterion, the contamination of field stars is estimated to be only 2 % (1a) and 10 % (1b), which is almost negligible. The number of resultant cluster members of Cloud 1a and Cloud 1b are 18 and 45, respectively. The radii of the defined cluster region in Cloud 1a and Cloud 1b are 1.1 pc (14'') and 2.2 pc (28''), respectively (see Figure 1). Therefore, the estimated stellar densities of the clusters are 5 pc^{-2} and 3 pc^{-2} , respectively. The achieved limiting magnitudes correspond to the mass-detection limit of $< 1 M_\odot$ for the kinematic distance ($D = 16$ kpc).

Figure 4 shows the K -band luminosity functions (KLFs), which are the number of stars as a function of K -band magnitude, for the member of two Cloud 1 clusters. The estimated completeness limit of Cloud 1 data is about $K_S = 20$ mag. We estimated the detection completeness by the number of field stars, which rapidly decrease at $K_S > 20$ mag. The KLF of the Cloud 1a cluster shows a rather stochastic curve probably because of the small number of detected members due to the large differential extinction, or the truly small number of members. Therefore, we use the KLF of the Cloud 1b cluster for the present study assuming that the Cloud 1a and 1b clusters have similar properties.

3.3. Molecular Clouds Distribution in Cloud 1

In the CO distribution of Cloud 1 (Figure 5), we detected two CO peaks (Cloud 1a and Cloud 1b) at $v_{\text{LSR}} \sim 100\text{ km s}^{-1}$ and a newly found bridge structure, which connects the two peaks. To estimate the masses of these clouds from the CO intensity I_{CO} , we used the same mass-calibration ratio $N(\text{H}_2)/I_{\text{CO}}$ as Digel et al. (1994) ($2.3 \times 10^{20}\text{ cm}^{-2} (\text{K km s}^{-1})^{-1}$; the Galactic average value). The estimated masses of Cloud 1a, Cloud 1b, and the bridge are 3.0×10^3 , 3.5×10^3 , and $4.5 \times 10^3 M_\odot$, respectively. The estimated velocity width of Cloud 1a, Cloud 1b, and the bridge are 2.2, 2.4, and 1.9 km s^{-1} , respectively. The estimated radii of Cloud 1a and Cloud 1b are 5.6 and 4.2 pc, respectively, and the length of the bridge is 42 pc. The parameters for Cloud 1a and Cloud 1b are consistent with the results of Digel et al. (1994).

Figure 5 also shows mid-infrared (MIR) pseudo color images from the *WISE* data around Cloud 1. We confirmed that the Cloud 1 clusters are also detected in the MIR images as groups of compact reddened stellar objects. We found some other compact reddened stellar ob-

jects around the two CO peaks and in the bridge, which also appear to be associated with Cloud 1. The large diffuse reddened ($12\text{ }\mu\text{m}$) structures are considered to be the Galactic cirrus (Meisner & Finkbeiner 2014) in the foreground.

3.4. Extinction Inside Cloud 1

We compared the extinction of the Cloud 1 clusters from our NIR data to that from the ^{13}CO column density in the literature. Ruffle (2006) estimated the ^{13}CO column density of Cloud 1a to be $N(^{13}\text{CO}) = 2.09 \pm 0.32 \times 10^{15}\text{ cm}^{-2}$, but no estimate was made for Cloud 1b. From this column density, we estimated the extinction of Cloud 1a to be $A_V = 4.4$ mag, assuming the same dust-to-gas ratio and ^{13}CO fractional abundance as the solar neighborhood (e.g., Frerking et al. 1982). The total extinction of Cloud 1a from our data is $A_V = 5 \sim 8$ mag (see the top right inset of Figure 3), and the extinction by foreground interstellar clouds at $R_G < 20$ kpc is estimated to be $A_V = 3 \sim 4$ mag (e.g., Amôres & Lépine 2005). Therefore, the extinction of the Cloud 1a clusters contributed from only the molecular cloud is estimated to be $A_V = 1 \sim 5$ mag. In view of the systematic uncertainties of related parameters, this value is roughly consistent with the extinction derived from the ^{13}CO data. Although the dust-to-gas ratio in such low-metallicity environment compared to the solar neighborhood is of great interest, it is hard to discuss the possible difference without other independent data.

3.5. H I Distribution around Cloud 1

The large-scale H I distribution around Cloud 1 (Figure 6) shows that there is an H I peak of the HVC Complex H (HVC 131+1-200) close to Cloud 1 on the sky with a separation of only $\sim 0.5^\circ$, though they are about 100 km s^{-1} apart from each other in the line-of-sight velocities. Furthermore, there is a large H I shell at $v_{\text{LSR}} \sim -100\text{ km s}^{-1}$, which was originally identified by Heiles (1979). Cloud 1 overlaps in position with part of the shell, at around $l \sim 131^\circ.1$, $b \sim 1^\circ.5$, and also in the line-of-sight velocity (Morras et al. 1998). The shell is elongated along the Galactic plane and its size is about $7^\circ \times 3.5^\circ$, approximately constant in the size and position within the v_{LSR} velocity range of -109 to -98 km s^{-1} , suggesting that the cavity surrounded by the shell has a cylindrical shape (Morras et al. 1998).

The high-resolution H I map around Cloud 1 from the CGPS data (see Figure 1) shows that Cloud 1 is associated with an elongated H I distribution in the same velocity range. We estimated the H I column density, radius, mass, and velocity width of the H I cloud as $3.6 \times 10^{20}\text{ cm}^{-2}$, 67 pc, $4.1 \times 10^4 M_\odot$, and 9.1 km s^{-1} , respectively.

4. PROPERTIES OF CLOUD 1 CLUSTERS

Because the slope and peak magnitude of KLF vary with age and distance (Muench et al. 2000), we estimate those parameters of the Cloud 1 clusters by comparing the observed KLF with that of the young (0.5–1 Myr) embedded cluster in the EOG, the Digel Cloud 2 clusters (Yasui et al. 2006, 2008). The photometric distance of Cloud 2 has been estimated to be $R_G = 15\text{--}19$ kpc ($D = 8\text{--}12$ kpc) by high-resolution optical spectroscopy

TABLE 2
PROPERTIES OF CLOUD 1 AND CLOUD 2

Cloud	Cloud Mass ($10^3 M_\odot$)	Number of Stars	Disk Fraction (%)	Age (Myr)	R_G (kinematic) (kpc)	R_G (photometric) (kpc)
Cloud 1a	3.0	18	14 ± 10 (2/14)	<1	22	≥ 19
Cloud 1b	3.5	45	24 ± 8 (9/37)	<1	22	≥ 19
Bridge	4.5	22	...
Cloud 2-S ^a	8.5	66	27 ± 7 (16/59)	0.5–1.0	23.6	19
Cloud 2-N ^a	14	72	9 ± 4 (5/52)	0.5–1.0	23.6	19

NOTE. — ^a The mass, kinematic distance, photometric distance of Cloud 2 clouds are from Digel et al. (1994), Stil & Irwin (2001), Kobayashi et al. (2008), respectively. Other parameters of Cloud 2 are estimated by Yasui et al. (2006, 2008, 2010).

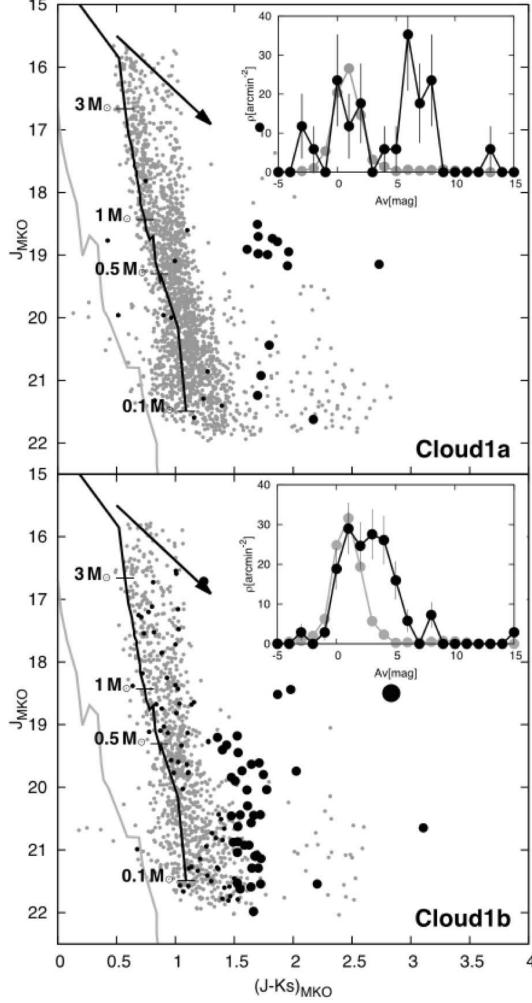


FIG. 3.— $(J - K_S)$ vs. J color-magnitude diagram for the Cloud 1 clusters in the MKO system. The top-right inset of each panel shows A_V distributions of stars in the cluster regions (black filled circles and lines) and in the field (gray filled circles and lines). The error bars show the uncertainties assuming Poisson statistics. The gray lines show dwarf tracks (Bessell & Brett 1988), while the black lines show isochrone models (1.0 Myr; Siess et al. 2000). The black arrows show the reddening vectors of $A_V = 5$ mag. The filled circles show stars in the cluster regions of Cloud 1a and Cloud 1b, respectively, small circles show field stars in the cluster regions, large circles show identified cluster members, and the very large circle shows the most luminous dereddened source. The gray dots show field stars in the field of view.

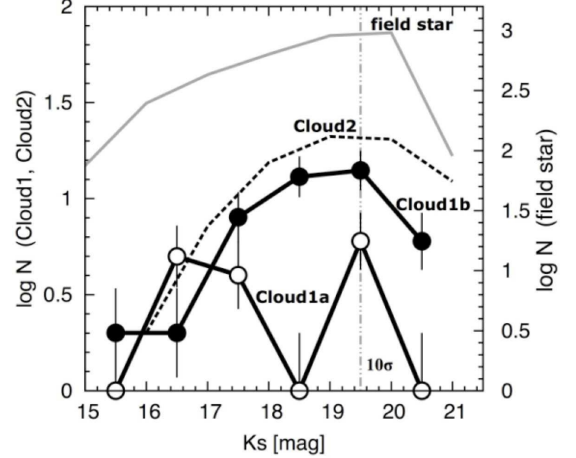


FIG. 4.— K-band luminosity function (KLF) of Cloud 1a (open circle), Cloud 1b (filled circle), and Cloud 2 (dashed line) clusters. The KLF for Cloud 2 is from the left panel of Figure 10 in Yasui et al. (2008). The error bars show the uncertainties assuming Poisson statistics. The gray line shows all of the field stars in the MOIRCS images of Cloud 1. The vertical dotted line shows the estimated completeness limit of Cloud 1 data (note that the completeness limit for Cloud 2 is about 20 mag).

of a B-type star MR1 (Smartt et al. 1996), which is apparently associated with Cloud 2 (de Geus et al. 1993); the shortest and longest distances are based on LTE and nonLTE model stellar atmospheres, respectively. Each producing errors are less than 15% ($D = 8 \pm 1$ – 12 ± 2 , $R_G = 15 \pm 1$ – 19 ± 2). In this paper, we adopt $R_G = 19$ kpc ($D = 12$ kpc) because the nonLTE model is more likely to be accurate for stars in the effective temperature regime of MR-1 (Smartt et al. 1996; Kobayashi et al. 2008) and also because $R_G = 15$ kpc has too much large discrepancy with $R_G = 22$ kpc from the kinematic distance. In Table 2, the properties of the Cloud 1 and 2 clusters are listed.

4.1. Age

We estimated the age using the slope of KLF, which is modeled to vary with age (Muench et al. 2000) and the slope becomes steeper with older age. Yasui et al. (2006, 2008) discussed the age of the Cloud 2 clusters by comparing observed KLF and model KLFs of various ages. They estimated the ages of the Cloud 2 clusters to be 0.5–1 Myr, and 2 Myr at most, because the model KLF of 0.1 Myr and 2 Myr have gentler and steeper slopes, respectively, than the observed KLF of the Cloud 2 clusters (see Figures 7 and 10 in Yasui et al. 2006 and 2008, respectively). Figure 4 shows that the KLF of

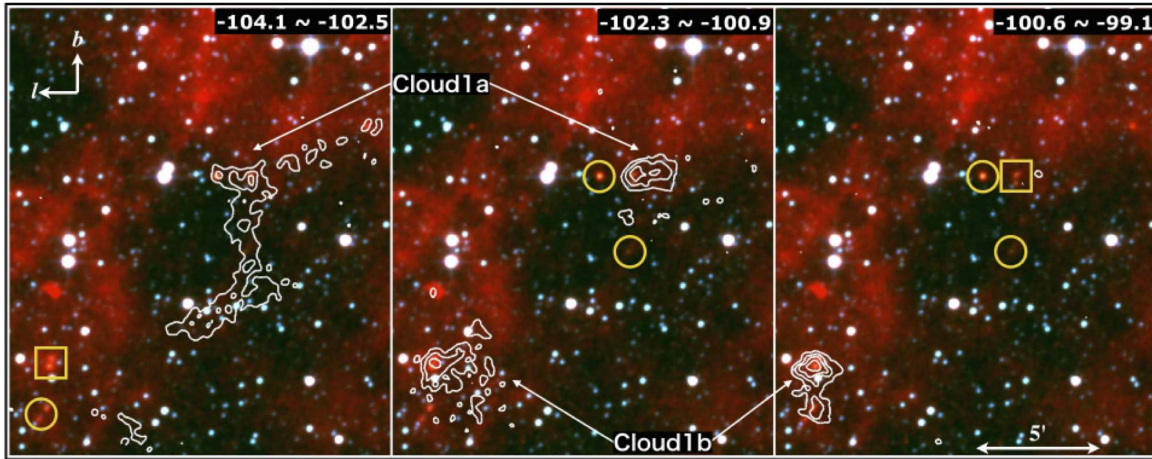


FIG. 5.— ^{12}CO velocity channel maps for three consecutive line-of-sight velocity ranges in km s^{-1} (from NRO 45 m telescope data) and mid-infrared pseudo color image around Cloud 1. The color images are produced by combining the 3.4, 4.6, and $12\ \mu\text{m}$ images from the *WISE* data. The yellow circles show compact reddened stellar objects in Cloud 1, and the yellow boxes show the Cloud 1a and 1b clusters, which are detected by the 8.2 m Subaru telescope. The contour interval is $0.46\ \text{K km s}^{-1}$ and range is from 0.46 to $1.82\ \text{K km s}^{-1}$.

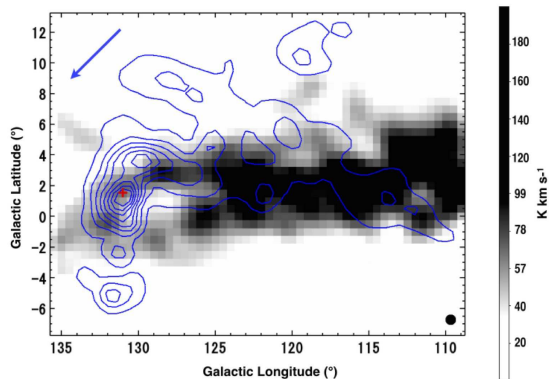


FIG. 6.— H I clouds in the extreme outer Galactic disk and HVC Complex H seen in a wide field from LAB data. While the blue contours show Complex H ($v_{\text{LSR}} = -229.8 \sim -150.5\ \text{km s}^{-1}$), the grayscale H I map shows the Galactic disk at $v_{\text{LSR}} = -104.1 \sim -98.9\ \text{km s}^{-1}$. The red cross marks the position of Cloud 1 in the Galactic disk ($v_{\text{LSR}} \sim -101\ \text{km s}^{-1}$). The contour interval is $10.8\ \text{K km s}^{-1}$ (20σ) and the range is from 8.5 to $73.1\ \text{K km s}^{-1}$ (15σ to 135σ). The blue arrow shows the direction of Complex H's motion (Lockman 2003). The black filled circle shows the beam size of the LAB data ($\sim 35'$).

the Cloud 1b and Cloud 2 clusters have a similar slope between $K_S = 16$ to $19\ \text{mag}$, and therefore, we estimated the age of the Cloud 1 clusters to be similar to the Cloud 2 clusters (0.5 – $1\ \text{Myr}$).

As an additional check of the age, we derived the disk fraction (DF) of the clusters, which is the percentage of cluster members with a optically thick circumstellar dust disk. Because the DF is known to decrease with increasing age up to $10\ \text{Myr}$ (e.g., Lada 1999; Haisch et al. 2001; Hernández et al. 2007; Yasui et al. 2010), it is sometimes used for the estimate of the cluster age. Following the description in Yasui et al. (2009, 2010), we derived the DF of the Cloud 1 clusters using the $H-K_S$ versus $J-H$ color-color (CC) diagram. The resulting DF of $24 \pm 8\%$ ($9/37$) for detected sources with $S/N > 10\sigma$ suggests that the age of the Cloud 1 clusters is less than $1\ \text{Myr}$ assuming the rapidly decaying DF curve in the low-metallicity environment (Figure 1 in Yasui et al. 2010). Because the ages estimated from both KLF and DF are consistent, we conclude that the

age of the Cloud 1 clusters is less than $1\ \text{Myr}$, suggesting that these clusters are truly young embedded clusters.

4.2. Photometric Distance

The peak magnitude of KLF is sensitive to age and distance of the cluster. For older age and larger distance, the peak magnitude becomes fainter. Figure 4 shows that the peak magnitude of the Cloud 1b cluster is similar to or fainter than, that of the Cloud 2 cluster. In view of the similarity of the age of the Cloud 2 cluster (see Section 4.1), the Cloud 1 clusters are expected to have the same or larger distance than the Cloud 2 cluster. Therefore, the distance to the Cloud 1 clusters with R_G is suggested to be more than $19\ \text{kpc}$ ($D \geq 12\ \text{kpc}$), which is consistent with the kinematic distance ($R_G = 22\ \text{kpc}$; Digel et al. 1994). In addition, we tried to estimate the distance to the Cloud 1 clusters, assuming that the most luminous star in the cluster is Herbig Ae/Be star of 3 – $5\ M_\odot$, which is suggested for such small clusters (Testi et al. 1999; Weidner & Kroupa 2006). The resultant distance is $8\ \text{kpc} \leq D \leq 21\ \text{kpc}$ ($15\ \text{kpc} \leq R_G \leq 27\ \text{kpc}$), which is consistent with the estimated distance by KLF and kinematic distance. Therefore, we suggest that the Cloud 1 clusters are located in the EOG region.

5. POSSIBLE TRIGGERED CLOUD/STAR FORMATION IN CLOUD 1

Cloud/star formation in a low-density environment, such as the EOG, is of strong interest in connection to the star formation in the early phase of the formation of the Galaxy (Kobayashi et al. 2008). Because of the low-density, triggered formation as opposed to spontaneous formation may play a crucial role in such an environment (Elmegreen 2011, 2012). Triggered star formation on the scale of a molecular cloud is nominally described as follows (Elmegreen 1998, 2011), (1) stellar pressure (including expansion of H II region and supernova remnant (SNR) shell), and (2) collision and collapse between two clouds (cloud-cloud collision). In the following we introduce the unique environment of Cloud 1 to discuss the possibility that a *large-scale* cloud-cloud collision, which was originally proposed by Morras et al. (1998), is

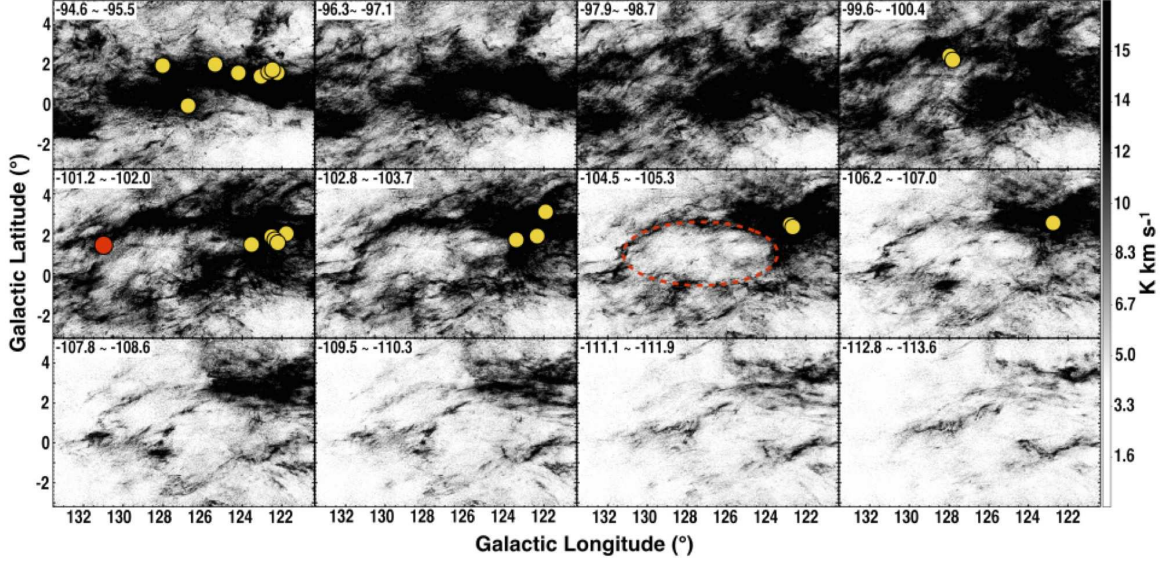


FIG. 7.— H I channel map from the CGPS data. Every other channel between -94 and -113 km s^{-1} is shown. The red filled circle shows the position of Cloud 1, and the dotted red line traces the large shell structure (see Section 3.4, Section 5.1). The yellow filled circles show the positions of the molecular clouds, which are identified in the FCRAO data (see Section 5.1 for detail).

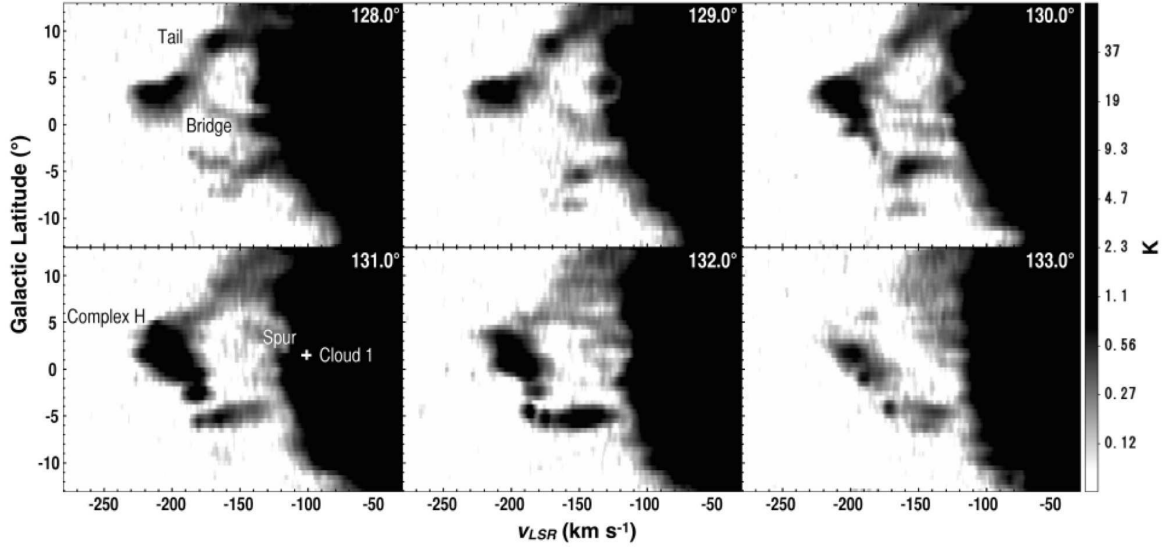


FIG. 8.— H I velocity-latitude cut through Cloud 1 from $l = 128.0^\circ$ to 133.0° made from the LAB data. The white cross shows the position of Cloud 1. Besides the probable tidal-interaction “tail” (Lockman 2003), some other “bridge” or “spur” features are seen in between the Complex H ($v_{\text{LSR}} \sim -200$ km s^{-1}) and the Galactic disk ($v_{\text{LSR}} \leq -100$ km s^{-1}).

the trigger of cloud/star formation of Cloud 1.

5.1. Large H I Shell

Cloud 1 is located on a large H I shell with a size of $0.8 \text{ kpc} \times 0.9 \text{ kpc}$ at the kinematic distance of $R_G = 22$ kpc (Figure 6, see also Section 3.4). Therefore, the star-formation mechanism is primarily suggested to be connected to the shell formation. In fact, such a large-scale triggered star formation by a super bubble or a super shell is reported for several regions in the Local arm (e.g., Lee & Chen 2009), the Perseus arm (e.g., Sakai et al. 2014; Lee & Lim 2008), and the EOG (Kobayashi et al. 2008). In addition to Cloud 1, we noticed several more molecular clouds, which are associated with the shell, from the list of molecular clouds identified in the FCRAO data (Brunt et al. 2003). Because no molecular cloud is

found inside or outside the shell (see Figure 7), we suggest that all those clouds are related to the shell formation. We will discuss the star formation activity in those clouds elsewhere in the future.

5.2. Stellar Feedback?

First, we discuss the possibility that the shell formation was triggered by stellar feedback. Morras et al. (1998) estimated the energy required to produce the large H I shell by a sudden explosion is of the order of $\sim 10^{53}$ erg, which requires the combined action of stellar winds and supernova explosions. However, a large OB association, which can make such a large shell, has not been detected near Cloud 1 (Morras et al. 1998). To confirm this idea, we reexamined the presence of any prominent sources of stellar pressure inside the H I shell, using the

latest archival data compiled after Morras’s work : H α images (IPHAS), MIR images (*WISE*), and H I data (LAB and CGPS). However, we could not identify any source and/or structure that traces an OB association or an SNR.

5.3. HVC Impacting on the Galactic Disk?

Next, we pay attention to the interaction between Complex H and the Galactic disk, which was first noted by Morras et al. (1998) and later discussed by others (e.g., Blitz et al. 1999; Lockman 2003; Simon et al. 2006), to discuss if it can cause the H I shell formation as well as the molecular cloud/star formation. Based on H I data with the Effelsberg 100 m Radio Telescope, Morras et al. (1998) suggested the impact of an HVC on the outer Galactic disk, which resulted in the presently observed Complex H and the large H I shell. Based on highly sensitive data with the Green Bank Telescope, Lockman (2003) paid attention to the “tail” structure between Complex H and the Galactic disk in a position-velocity (PV) map, and suggested that the Complex H is more like a satellite of the Galaxy in an inclined retrograde orbit, whose outermost layers are currently being stripped away in its encounter with the Galaxy. However, in a PV map made from the LAB data (Figure 8), we have noticed that some intermediate velocity structures of the “spur” and “bridge”, which connect the Complex H to the Galactic disk, in addition to the “tail” structure, and that Cloud 1 appears to be located at the edge of such structures. Although the large-scale tail structure is likely to be formed by tidal force (Lockman 2003), the existence of the bridge and spur structures in the PV diagrams as well as the H I shell structure (Section 5.1) support the Morras et al. impacting idea because such structures are predicted by the simulation of cloud-cloud collision (e.g., Figure 2 in Comeron & Torra 1992).

Blitz et al. (1999) posed a major objection to the Morras et al. impacting idea because there is no trace of an impact, such as H α and X ray emission from a strong shock, suggesting that Complex H is an extragalactic H I cloud. Simon et al. (2006) followed the Blitz’s extragalactic idea to present the argument that Complex H is either a dark galaxy in the Local Group, or an example of a cold accretion flow onto the Galaxy. However, a similar case of an H I cloud impacting on the Galactic disk, which does not show any detectable H α or soft X-ray emission, is reported for HVC 306-2+230 by McClure-Griffiths et al. (2008), who argue that such emissions from associated ionized gas are absorbed by foreground dust and gas in the Galactic plane. The Complex H is also located at low-galactic latitude, and moderately high extinction is measured for the large distance. Therefore, the lack of H α and X ray emission does not appear to be strong evidence against Morras’ impacting idea.

We also considered the timescale of the collision (impact) in relation to the cloud/star formation in Cloud 1. Assuming that the H I peak of the Complex H has a spherical shape with a radius of $R \sim 1.4$ kpc (5° at $R_G = 22$ kpc) and the relative velocity of $\Delta v \sim 100$ km s $^{-1}$, the estimated dynamical timescale of the collision is $R/\Delta v \sim 10$ Myr. The typical timescale for formation of a molecular cloud is considered to be ~ 10 Myr (Ballesteros-Paredes et al. 2007; Gratier et al. 2012). The lifetime of a molecular cloud as well as the timescale of star formation is also considered as ~ 10 Myr (Mouschovias et al. 2006). All of these timescales are not longer than the estimated collision timescale. In fact, the ages of Cloud 1 clusters are estimated to be < 1 Myr (see Section 4.1). In all possible cases in which the impact triggered (1) both molecular cloud and star formation, (2) only molecular cloud formation, or (3) only star formation in Cloud 1, the collision timescale does not conflict with the timescales of subsequent processes.

Therefore, we suggest a possibility that the formation of the Cloud 1 clusters and Cloud 1 itself was triggered by the impact of Complex H on the Galactic disk at $R_G \sim 22$ kpc. Further study of this cloud will be very important for revealing the dynamical processes of such triggered formation.

6. SUMMARY

We present a detailed study of Digel Cloud 1, which is one of the farthest molecular clouds in the Galaxy, with the kinematically determined Galactocentric radius of ~ 22 kpc. Our main results are as follows.

1. With NIR imaging and ^{12}CO mapping that covers the entire Cloud 1, we detected two young embedded clusters located in two dense cores.
2. Using properties of the KLF and DF, we have estimated the age of the clusters to be < 1 Myr.
3. Using properties of the KLF and the above age, we have estimated the photometric distance of the clusters to be $D \geq 12$ kpc ($R_G \geq 19$ kpc), which is consistent with the kinematic distance.
4. Based on previous research on Complex H and the latest H I survey data (CGPS and LAB), we suggest that the impact of HVC Complex H onto the outer part of the Galactic disk could be the major trigger of Cloud 1 formation as well as star formation in Cloud 1.

We are grateful to the staff of the Subaru 8.2 m telescope, in particular, Ichi Tanaka for his dedicated support during and after the observation. We are also grateful to the staff of the NRO 45 m telescope. We thank the anonymous reviewer for a careful reading and thoughtful suggestions that significantly improved this paper.

REFERENCES

- Amôres, E. B., & Lépine, J. R. D. 2005, *AJ*, 130, 659
 Ballesteros-Paredes, J., Klessen, R. S., Mac Low, M.-M., & Vazquez-Semadeni, E. 2007, in *Protostars and Planets V*, ed. B. Reipurth, D. Jewitt, & K. Keil (Tucson, AZ: Univ. Arizona Press), 63
 Bessell, M. S., & Brett, J. M. 1988, *PASP*, 100, 1134
 Blitz, L., Spergel, D. N., Teuben, P. J., Hartmann, D., & Burton, W. B. 1999, *ApJ*, 514, 818
 Brunt, C. M., Kerton, C. R., & Pomerleau, C. 2003, *ApJS*, 144, 47
 Comeron, F., & Torra, J. 1992, *A&A*, 261, 94
 de Geus, E. J., Vogel, S. N., Digel, S. W., & Gruendl, R. A. 1993, *ApJL*, 413, L97
 Digel, S., de Geus, E., & Thaddeus, P. 1994, *ApJ*, 422, 92

- Drew, J. E., Greimel, R., Irwin, M. J., et al. 2005, *MNRAS*, 362, 753
- Elmegreen, B. G. 1998, in *ASP Conf. Ser. 148, Origins*, ed. C. E. Woodward, J. Michael Shull, & H. A. Thronson, Jr. (San Francisco, CA: ASP), 150
- Elmegreen, B. G. 2011, *EAS Publications Series*, Vol. 51, 45
- Elmegreen, B. G. 2012, in *IAU Symp. 284, The Spectral Energy Distribution of Galaxies*, ed. R. J. Tuffs & C. C. Popescu (Cambridge: Cambridge Univ. Press), 317
- Emerson, D. T., & Graeve, R. 1988, *A&A*, 190, 353
- Frerking, M. A., Langer, W. D., & Wilson, R. W. 1982, *ApJ*, 262, 590
- Gratier, P., Braine, J., Rodriguez-Fernandez, N. J., et al. 2012, *A&A*, 542, A108
- Haisch, K. E., Jr., Lada, E. A., & Lada, C. J. 2001, *ApJL*, 553, L153
- Heiles, C. 1979, *ApJ*, 229, 533
- Hernández, J., Hartmann, L., Megeath, T., et al. 2007, *ApJ*, 662, 1067
- Heyer, M. H., Brunt, C., Snell, R. L., et al. 1998, *ApJS*, 115, 241
- Heyer, M. H., Carpenter, J. M., & Snell, R. L. 2001, *ApJ*, 551, 852
- Ichikawa, T., Suzuki, R., Tokoku, C., et al. 2006, *Proc. SPIE*, 6269,
- Kalberla, P. M. W., Burton, W. B., Hartmann, D., et al. 2005, *A&A*, 440, 775
- Kerp, J., Mack, K.-H., Egger, R., et al. 1996, *A&A*, 312, 67
- Kobayashi, N., & Tokunaga, A. T. 2000, *ApJ*, 532, 423
- Kobayashi, N., Yasui, C., Tokunaga, A. T., & Saito, M. 2008, *ApJ*, 683, 178
- Lada, E. A. 1999, *NATO ASIC Proc. 540: The Origin of Stars and Planetary Systems*, 441
- Lada, C. J., & Adams, F. C. 1992, *ApJ*, 393, 278
- Lada, C. J., & Lada, E. A. 2003, *ARA&A*, 41, 57
- Lee, H.-T., & Chen, W. P. 2009, *ApJ*, 694, 1423
- Lee, H.-T., & Lim, J. 2008, *ApJ*, 679, 1352
- Leggett, S. K., Currie, M. J., Varricatt, W. P., et al. 2006, *MNRAS*, 373, 781
- Lockman, F. J. 2003, *ApJL*, 591, L33
- McClure-Griffiths, N. M., Staveley-Smith, L., Lockman, F. J., et al. 2008, *ApJ*, 673, L143
- Meisner, A. M., & Finkbeiner, D. P. 2014, *ApJ*, 781, 5
- Morras, R., Bajaja, E., & Arnal, E. M. 1998, *A&A*, 334, 659
- Mouschovias, T. C., Tassis, K., & Kunz, M. W. 2006, *ApJ*, 646, 1043
- Muench, A. A., Lada, E. A., & Lada, C. J. 2000, *ApJ*, 533, 358
- Rieke, G. H., & Lebofsky, M. J. 1985, *ApJ*, 288, 618
- Ruffle, P. 2006, PhD thesis
- Sakai, N., Sato, M., Motogi, K., et al. 2014, *PASJ*, 66, 3
- Sawada, T., Ikeda, N., Sunada, K., et al. 2008, *PASJ*, 60, 445
- Siess, L., Dufour, E., & Forestini, M. 2000, *A&A*, 358, 593
- Simon, J. D., Blitz, L., Cole, A. A., Weinberg, M. D., & Cohen, M. 2006, *ApJ*, 640, 270
- Smartt, S. J., Dufton, P. L., & Rolleston, W. R. J. 1996, *A&A*, 305, 164
- Smartt, S. J., & Rolleston, W. R. J. 1997, *ApJ*, 481, L47
- Snell, R. L., Carpenter, J. M., & Heyer, M. H. 2002, *ApJ*, 578, 229
- Stil, J. M., & Irwin, J. A. 2001, *ApJ*, 563, 816
- Sunada, K., Yamaguchi, C., Nakai, N., et al. 2000, *Proc. SPIE*, 4015, 237
- Taylor, A. R., Gibson, S. J., Peracaula, M., et al. 2003, *AJ*, 125, 3145
- Testi, L., Palla, F., & Natta, A. 1999, *A&A*, 342, 515
- Tokunaga, A. T., Simons, D. A., & Vacca, W. D. 2002, *PASP*, 114, 180
- Wakker, B. P. 1991, *A&AS*, 90, 495
- Wakker, B. P., & Schwarz, U. J. 1991, *A&A*, 250, 484
- Weidner, C., & Kroupa, P. 2006, *MNRAS*, 365, 1333
- Wolfire, M. G., McKee, C. F., Hollenbach, D., & Tielens, A. G. G. M. 2003, *ApJ*, 587, 278
- Wright, E. L., Eisenhardt, P. R. M., Mainzer, A. K., et al. 2010, *AJ*, 140, 1868
- Yamaguchi, C., Sunada, K., Iizuka, Y., Iwashita, H., & Noguchi, T. 2000, *Proc. SPIE*, 4015, 614
- Yasui, C., Kobayashi, N., Tokunaga, A. T., Saito, M., & Tokoku, C. 2009, *ApJ*, 705, 54
- Yasui, C., Kobayashi, N., Tokunaga, A. T., Saito, M., & Tokoku, C. 2010, *ApJ*, 723, L113
- Yasui, C., Kobayashi, N., Tokunaga, A. T., Terada, H., & Saito, M. 2006, *ApJ*, 649, 753
- Yasui, C., Kobayashi, N., Tokunaga, A. T., Terada, H., & Saito, M. 2008, *ApJ*, 675, 443